




## Article

# Photocatalytic Properties of Immobilised Graphitic Carbon Nitride on the Alumina Substrate

Milan Vukšić <sup>1,\*</sup> , Martina Kocijan <sup>1,\*</sup> , Lidija Čurković <sup>1</sup> , Tina Radošević <sup>2</sup>, Damjan Vengust <sup>3</sup> and Matejka Podlogar <sup>2,4</sup>

<sup>1</sup> Department of Material, Faculty of Mechanical Engineering and Naval Architecture, University of Zagreb, Ivana Lučića 5, 10000 Zagreb, Croatia

<sup>2</sup> Department for Nanostructured Materials, Jožef Stefan Institute, Jamova Cesta 39, SI-1000 Ljubljana, Slovenia

<sup>3</sup> Advanced Materials Department, Jožef Stefan Institute, Jamova Cesta 39, SI-1000 Ljubljana, Slovenia

<sup>4</sup> Faculty of Chemistry and Chemical Technology, University of Ljubljana, Večna Pot 113, SI-1000 Ljubljana, Slovenia

\* Correspondence: milan.vuksic@fsb.hr (M.V.); martina.kocijan@fsb.hr (M.K.)

**Abstract:** Textile industries significantly impact the contamination of wastewater. Conventional wastewater treatment methods consider the most common pollutants; however, they are very expensive and commonly produce toxic by-products. In the scientific community, advanced oxidation processes appear to be the most appealing, and a majority of the published work considers heterogeneous photocatalysis for the degradation of various toxic chemicals. For convenience, the reaction is performed directly in the water environment. In this work, a metal-free graphitic carbon nitride (g-C<sub>3</sub>N<sub>4</sub>) was prepared through a simple thermal method using urea as a precursor. Prepared g-C<sub>3</sub>N<sub>4</sub> was deposited on the surface of the alumina ceramic ring by the dip-coating method using ethylene glycol as binder. The alumina ceramic ring, as substrate, was prepared by the slip casting method. Photocatalytic properties of immobilised graphitic carbon nitride were used for degradation of methylene blue as a model pollutant under simulated solar light irradiation. The photocatalyst was characterised by XRD, FTIR, UV-Vis DRS, TGA, BET and SEM/EDX analyses. The photocatalytic degradation of MB from an aqueous solution was found to increase with increasing irradiation time. It was found that the graphitic carbon nitride immobilised on alumina ceramic is convenient for largescale environmental applications because the whole setup is cheap, nontoxic, easy to operate and offers reusability with a high removal rate of MB after three consecutive cycles.

**Keywords:** graphitic carbon nitride; alumina ceramic; photocatalysis; methylene blue



**Citation:** Vukšić, M.; Kocijan, M.; Čurković, L.; Radošević, T.; Vengust, D.; Podlogar, M.

Photocatalytic Properties of Immobilised Graphitic Carbon Nitride on the Alumina Substrate. *Appl. Sci.* **2022**, *12*, 9704. <https://doi.org/10.3390/app12199704>

Academic Editor: Antonio Miotello

Received: 20 August 2022

Accepted: 23 September 2022

Published: 27 September 2022

**Publisher's Note:** MDPI stays neutral with regard to jurisdictional claims in published maps and institutional affiliations.



**Copyright:** © 2022 by the authors. Licensee MDPI, Basel, Switzerland. This article is an open access article distributed under the terms and conditions of the Creative Commons Attribution (CC BY) license (<https://creativecommons.org/licenses/by/4.0/>).

## 1. Introduction

Pollution in oceans, lakes and rivers has become a global environmental burden. The presence of manmade organic species such as fertilizers, pesticides, and pharmaceuticals were found throughout all aquatic ecosystems [1]. One of the most frequent forms of pollution worldwide is dye contamination most abundantly generated by the industrial sector responsible to produce leather, textile, and cosmetics. Daily release of various raw materials such as cotton, synthetic fibres, and dyes pollutes the ecosystem. Bigger fragments are increasingly more often isolated by filtering and subsequently discarded in the land fields. Dyes and pigments remain due to their small molecular size and complex chemical structure [2,3]. The pollutants are abundant in water systems, where they degrade to simpler molecules by very complex physical and chemical mechanisms. One of those mechanisms is photolysis, where light irradiates a given volume of the mixture, thus providing a constant inflow of energy, which is responsible for scissoring chemical bonds.

On the laboratory scale, the process under consideration can be greatly enhanced. In the experiment, photocatalysts are usually considered. Heterogeneous photocatalysis uses solid-state catalyst immersed in 'polluted' water. Among them, graphitic carbon

nitride ( $g\text{-C}_3\text{N}_4$ ) gains considerable attention [4–6]. To evaluate the catalytic activity of heterogeneous catalysts it is convenient to disperse unsupported, bulk catalyst in a powder form in the targeted solution. In this way, it is possible to quickly gain information about its activity. However, from the application point of view, the catalyst should be immobilised on a suitable substrate such as ceramic [7,8], polymers [9,10], and zeolite [11,12]. Robust substrate with immobilised photocatalysts provide a stable system during a dynamic exchange of solution. Without any post-treatment, e.g., such as filtration or sedimentation to separate solution from the catalyst, they can be used sequentially multiple times. Immobilisation of the given catalyst also requires new research with respect to its physical and chemical properties. While the most important parameter such as its bandgap energy is not expected to change, the construction of a more complex setup brings about many other discrepancies. Among them, for example, is the scattering of the harvested light. Differences appear between for example isolated dispersed particles in sizes of a few 100 nm or deposited ones, because the former favour the light scattering over the desired absorption [13]. There are a lot of new parameters that must be considered when immobilising a given photocatalyst [14]. These issues are being continuously addressed. Novel insight is needed to prepare immobilised photocatalysts deposited together with noble metals, which were proven many times to improve activity [15,16], morphologically modified photocatalysts [17,18], and new strategies for the preparation of composites [19–21].

Graphitic carbon nitride has excellent properties with great potential to be used as a metal-free catalyst in wastewater treatment. The published scientific papers pursued the research in suspensions which has significant drawbacks such as toxicity of the nanoparticles, the uncontrolled release into the environment needs to be closely monitored. Many existing slurry-type reactors use nanoparticles suspension where separation and reuse of catalyst from the final product are difficult to achieve. Immobilised  $g\text{-C}_3\text{N}_4$  in the form of coating is a promising solution that opens the possibility of manufacturing reactors for reusable photocatalysis with reduced erosion of nanoparticles into the environment. Ceramic substrates are widely used due to their chemical stability, and very good mechanical properties. Alumina stands out among them. It is environmentally benign, inexpensive and can be easily envisioned even in high concentrated effluents [22,23]. It is stable at various temperature conditions and chemically very inert. In the presented study, the  $g\text{-C}_3\text{N}_4$  photocatalyst was deposited on such alumina substrate. The quality of  $g\text{-C}_3\text{N}_4$  coatings on ceramic substrates had a key role in efficient catalytic processes. The photocatalytic activity was evaluated by decolourisation of MB dye as well as degradation of the aromatic ring under simulated sunlight irradiation.

## 2. Materials and Methods

### 2.1. Materials

Urea ( $\geq 99\%$ ) and ethylene glycol ( $>99.5$ ) were purchased from Merck KGaA (Darmstadt, Germany). Methylene blue (MB) was supplied by VWR Chemicals GmbH (Dresden, Germany). Alumina powder and Tiron<sup>®</sup> were purchased from Almatix (Ludwigshafen, Germany) and Sigma-Aldrich (Steinheim, Germany), respectively. The ultra-pure water was produced in a LaboStar<sup>®</sup> PRO water purification system (resistivity 18.2 M $\Omega$ /cm at 24.5 °C, 0.2  $\mu\text{m}$  sterile filter, Siemens). The characteristics of the alumina powder are given in Table 1.

**Table 1.** The properties of the alumina powder provided by the manufacturer.

Chemical Composition (%)					
Na <sub>2</sub> O	Fe <sub>2</sub> O <sub>3</sub>	MgO	SiO <sub>2</sub>	CaO	Al <sub>2</sub> O <sub>3</sub>
0.07	0.02	0.05	0.03	0.02	rest
Physical and Ceramic Properties					
BET (m <sup>2</sup> g <sup>−1</sup> )	d <sub>90</sub> ( $\mu\text{m}$ )	d <sub>50</sub> ( $\mu\text{m}$ )	Green dens. (g cm <sup>−3</sup> )	Sintered dens. (g cm <sup>−3</sup> )	Shrinkage %
8.9	2	0.5	2.2 ± 0.1	3.93 ± 0.05	18.5 ± 0.7

## 2.2. Preparation of Alumina Substrate

The alumina ceramic ring was prepared by the slip casting method and used as the substrate for the deposition of synthesized  $g\text{-C}_3\text{N}_4$  catalyst. The stable alumina ceramic suspension (40 vol.%) was prepared by adding alumina powder (A 16 SG) and dispersant Tiron<sup>®</sup> into demineralised water. Afterward, all components were mixed for 2 h in the planetary ball mill (PM400, Retsch, Haan, Germany), poured into ring paster moulds, and dried at ambient temperature for 24 h. The ring-shaped green bodies were sintered applying the  $4\text{ }^\circ\text{C min}^{-1}$  heating rate till  $1650\text{ }^\circ\text{C}$  with a holding time of 6 h. The sintered ring-shaped alumina substrates with the following dimensions: inner diameter of  $25 \pm 2$  mm, outer diameter of  $55 \pm 2$  mm, and  $5 \pm 2$  mm thickness was obtained.

## 2.3. Preparation of $g\text{-C}_3\text{N}_4$

The graphitic carbon nitride photocatalyst was synthesised by heating urea as a precursor in a covered crucible. In a typical synthesis, 10 g of urea were heated up to  $550\text{ }^\circ\text{C}$  at a rate of  $5\text{ }^\circ\text{C/min}$  in an air atmosphere and left for 2 h to dwell in a chamber furnace (Nabertherm, Lilienthal, Germany). The obtained  $g\text{-C}_3\text{N}_4$  was cooled naturally to room temperature, and it was in the form of a light yellowish powder as shown in Figure 1.

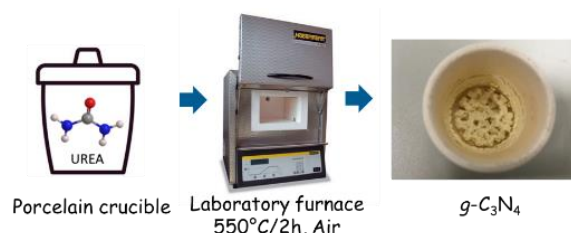


**Figure 1.** The obtained light yellowish bulk of  $g\text{-C}_3\text{N}_4$ .

## 2.4. Immobilisation of $g\text{-C}_3\text{N}_4$ on Alumina Substrate

The obtained  $g\text{-C}_3\text{N}_4$  catalyst was immobilised on an alumina substrate using a procedure previously reported [24]. The prepared  $g\text{-C}_3\text{N}_4$  catalyst and ethylene glycol were mixed in the appropriate ratio. The mixture was stirred for 15 min and transferred into an ultrasonic bath for 15 min at room temperature to obtain a homogeneous suspension. For the immobilisation of the catalyst on the alumina substrate, a dip-coating method was used. The alumina substrate was immersed in the catalyst suspension for 2 min and the photocatalyst adhered to the surface of the alumina substrate. Afterward, it was thermally treated in a dryer at  $105\text{ }^\circ\text{C}$  for 15 min. The immobilised  $g\text{-C}_3\text{N}_4$  catalyst on alumina support is shown in Figure 2.



**Figure 2.** Picture of immobilised  $g\text{-C}_3\text{N}_4$  catalyst on alumina substrate.

## 2.5. Characterisation of Prepared $g\text{-C}_3\text{N}_4$

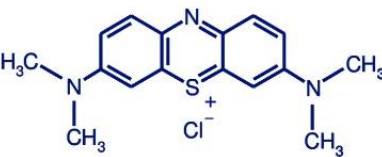
Morphology, chemical elemental composition, and surface analysis were conducted with a scanning electron microscope with energy dispersive spectroscopy (SEM/EDXS, Verios 4G HP, Thermo Fisher). To provide information related to the specific functional groups, the Fourier transform infrared spectroscopy-attenuated total reflectance (FTIR-ATR, Shimadzu, Kyoto, Japan) measurements were performed in the  $400\text{--}4000\text{ cm}^{-1}$  range at room temperature. UV-Vis diffuse reflectance spectra (DRS) were obtained in the measurement range of  $200\text{--}700\text{ nm}$  at room temperature. The samples were analysed

with a UV-3600 spectrophotometer (Shimadzu, Kyoto, Japan) equipped with a reflectance sphere using BaSO<sub>4</sub> as a reference. TGA analysis was performed with NETZSCH STA 449 C/6/G Jupiter—QMS 403 in the range from room temperature to 900 °C with the 5°/min heating rate. The N<sub>2</sub> adsorption–desorption isotherm and pore-size distribution of as-prepared g-C<sub>3</sub>N<sub>4</sub> photocatalyst was analysed using Brunauer–Emmett–Teller (BET) method (Quantachrome Nova 2000e, Anton Paar QuantaTec Inc., Graz, Austria). The crystallinity phase and composition of the prepared g-C<sub>3</sub>N<sub>4</sub> were obtained by an X-ray diffractometer (X'Pert PRO high-resolution X-ray diffractometer; PANalytical B.V., Almelo, Netherlands) using CuKα as a radiation source ( $\lambda = 1.5406 \text{ \AA}$ ) at  $2\theta$  ranging from 8° to 80° with the step of 0.033°/100 s.

## 2.6. Photocatalytic Tests

To examine the photocatalytic activity of the immobilised photocatalyst g-C<sub>3</sub>N<sub>4</sub>, the photodegradation of the MB dye (Table 2) with a concentration of 10 mg·L<sup>−1</sup> was investigated under simulated solar light irradiation. Osram's Ultra Vitalux lamp (300 W) was used as a light source. The MB dye aqueous solution and immobilised g-C<sub>3</sub>N<sub>4</sub> photocatalyst were stirred in the dark for 30 min to achieve an adsorption-desorption equilibrium between the organic pollutant and the photocatalyst. All the photocatalytic experiments were carried out under the same conditions at room temperature. At defined intervals, 15 min, the absorbance was monitored by UV-Vis spectroscopy on a Lambda 950 UV/VIS/NIR spectrophotometer (PerkinElmer, Waltham, MA, USA) in the 200–750 nm range using a quartz cuvette (Hellma Analytics, Stuttgart, Germany) with a path length of 10 mm. Under identical experimental conditions, the activity of bare alumina substrate was also investigated and compared with immobilised photocatalyst g-C<sub>3</sub>N<sub>4</sub> on the substrate.

**Table 2.** Physico-chemical properties of the understudied organic pollutant MB dye.

Organic pollutant	Methylene blue
IUPAC name	3,7-bis(dimethylamino)-phenothiazin-5-ium chloride
Chemical formula	C <sub>16</sub> H <sub>18</sub> ClN <sub>3</sub> S
Molar mass/g·mol <sup>−1</sup>	319.85
Chemical structure	

The kinetics study of MB photocatalytic decolourisation and degradation is described by pseudo-first-order kinetic equation. The integrated form of the pseudo-first-order kinetic model is expressed in Equation (1) [25]:

$$\ln(A_0/A_t) = k \cdot t \quad (1)$$

where  $A_0$  and  $A_t$  express the initial and remaining MB dye absorbance for a specific interval of time and  $k$  represents the first-order rate constant (min<sup>−1</sup>) of photocatalytic degradation of MB dye.

To investigate the reusability of immobilised g-C<sub>3</sub>N<sub>4</sub> catalyst, recycling experiments were carried out for three cycles under the same experimental conditions. After each cycle, the immobilised g-C<sub>3</sub>N<sub>4</sub> catalyst was washed with ultrapure water and ethanol, and then dried at 60 °C.

## 3. Results and Discussion

### 3.1. Catalyst Characterisation

Alumina substrate densification is well covered in the literature, and a process for the production of various alumina objects and crucibles has been commercialised within our institution, yielding a fully densified corundum ( $\alpha$ -Al<sub>2</sub>O<sub>3</sub>) phase. Synthesis of g-C<sub>3</sub>N<sub>4</sub>

is subtler especially if we consider small changes, which could influence the electronic structure and with-it photocatalytic activity.

The crystal structure was studied first by XRD, and the corresponding pattern of  $g\text{-C}_3\text{N}_4$  is presented in Figure 3A. The diffractogram shows two characteristic diffraction peaks at  $13.3^\circ$  (100) and  $27.5^\circ$  (002), which correspond to the in-plane spacing of repeated tri-s-triazine rings and the interlayer stacking reflection, respectively [26]. The spectrum is broad due to the small crystal size and reflects the sheet-like (2D) morphology of the material. This is evident because the (002) peak corresponding to interlayer stacking dominates the spectrum. Equivalently, because these planes represent the majority of the total and are parallel with the XRD sample holder, they provide more signals in a standard X-ray powder diffraction configuration setup. A slight elevation of the whole spectra could point out to a presence of less crystalline phase; however, if the 2D sheet is very thin, similar features would also be found.

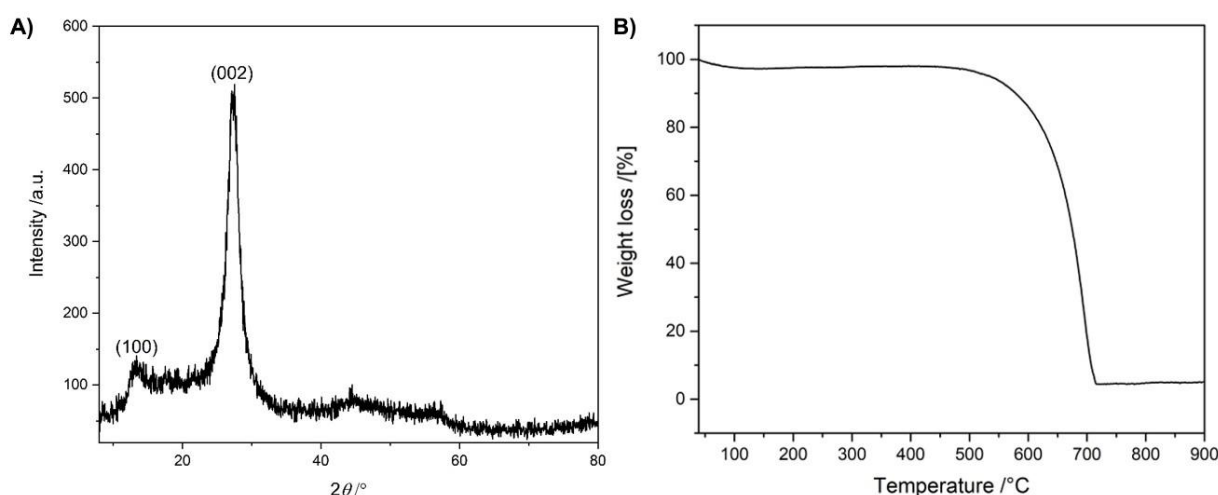


**Figure 3.** (A) X-ray diffractogram and (B) TGA analysis of  $g\text{-C}_3\text{N}_4$ .

The decomposition of  $g\text{-C}_3\text{N}_4$  powder measured by TGA analysis nicely follows expected temperature dependence (Figure 3B). There are no bumps that would indicate the presence of impurities [27]. According to evolved gas analysis (not shown), a small decrease in mass at 100  $^\circ\text{C}$  correspond to water loss, while in the degradation region also  $\text{CO}_2$  and  $\text{N}_2$  were detected. The degradation is completed at around 700  $^\circ\text{C}$ . Optical properties of the prepared  $g\text{-C}_3\text{N}_4$  were characterised by UV-visible diffuse reflection spectrum (UV-vis DRS) in Figure 4A. This semiconductor catalyst is supposed to be effective in simulated solar irradiation because  $g\text{-C}_3\text{N}_4$  absorbs light from the UV to the visible region, with slight variations with respect to the doping or shape of the crystals [28]. Utilizing Kubelka–Munk transformation (Figure 4B), the  $E_g$  value of 2.62 eV was estimated, which is similar to other reports and corresponds to an absorption edge starting in blue at 473 nm and extending to the UV region.

The fingerprint vibrational spectrum, which corresponds to specific chemical bonding in molecules was measured with FTIR, as shown in Figure 5. Normal modes of bond vibrations for  $g\text{-C}_3\text{N}_4$  can be easily identified. Most characteristics are those in the range between 1100–1700  $\text{cm}^{-1}$ . The strong peaks observed at approximately 1228, 1311, 1393, and 1456  $\text{cm}^{-1}$  correspond to the aromatic C–N stretching vibrations, whereas the heterocycles C=N stretching vibrations are found at 1539 and 1627  $\text{cm}^{-1}$  [29,30]. The typical peak of 805  $\text{cm}^{-1}$  represents the tri-s-triazine structure. The broad peaks located at 3000–3300  $\text{cm}^{-1}$  are assigned to the stretching of N–H and C–H bonds.



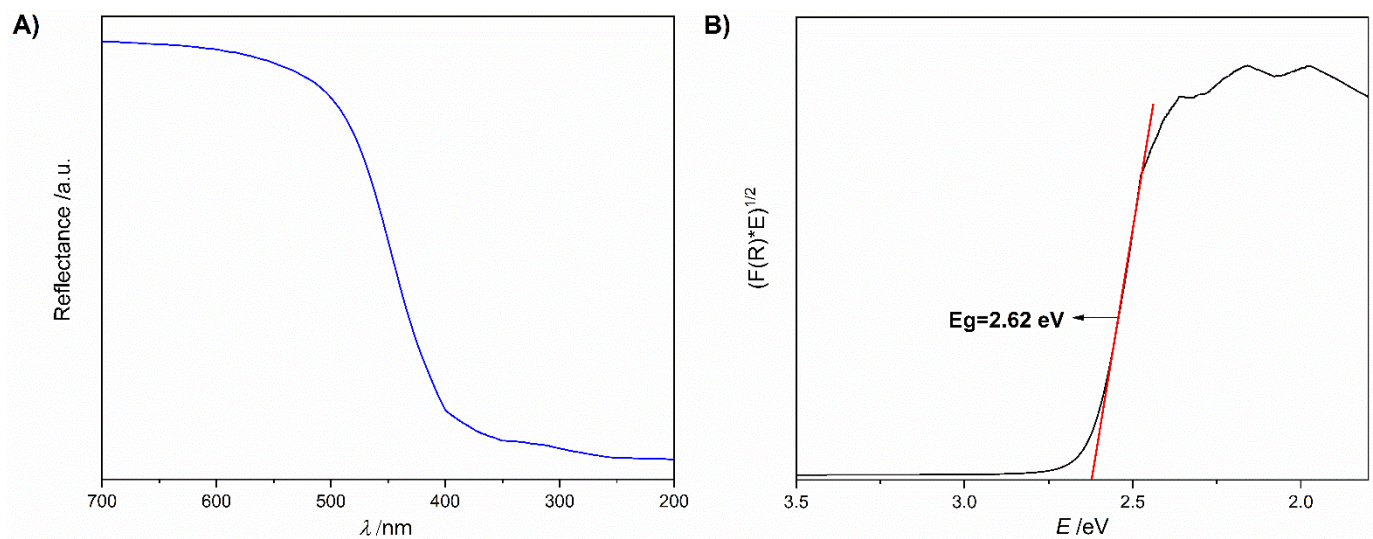


**Figure 4.** (A) UV-Visible diffuse reflectance spectra and (B) Kubelka–Munk transferred diffuse reflectance spectra of  $g\text{-C}_3\text{N}_4$ .

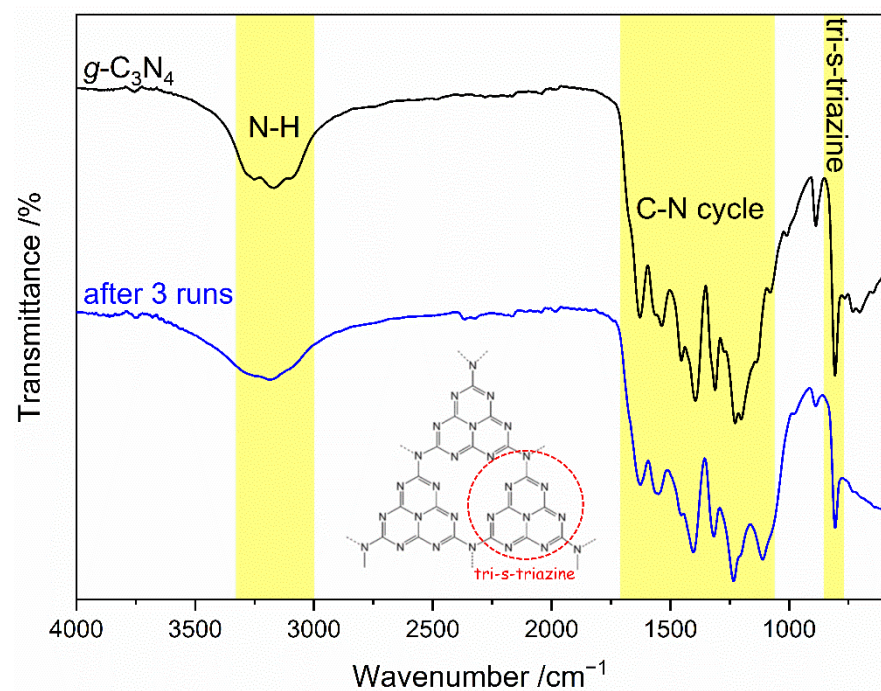


**Figure 5.** FTIR patterns of  $g\text{-C}_3\text{N}_4$ .

In contrast to other methods, the FTIR spectrum also revealed changes in the  $g\text{-C}_3\text{N}_4$  sample after catalytic treatment. The sample which was repeatedly exposed to the reaction (as revealed later) exhibited few differences. Most apparent is the loss of sharpness of individual peaks. It is clearly evident in the extra vibrational region between 3000–3300  $\text{cm}^{-1}$ , although not directly related to the  $g\text{-C}_3\text{N}_4$  structure, it is commonly found in this compound, [29,30] and can be associated with  $\text{H}_2\text{O}$  absorption and possible N-H bonds at the surface. In this particular region also C-H vibrations are revealed [30,31] and could similarly be associated with the surface changes.

Microscopic analysis of the prepared photocatalyst is presented in Figure 6A.  $g\text{-C}_3\text{N}_4$  appear curled, banded, and twisted and range in sizes from 0.5 to 1.5  $\mu\text{m}$ . Thickness is hard to determine; however, it is much less than 100 nm. EDX which was also performed show the right ratio between carbon and nitrogen within expectation (inset Figure 6 B).

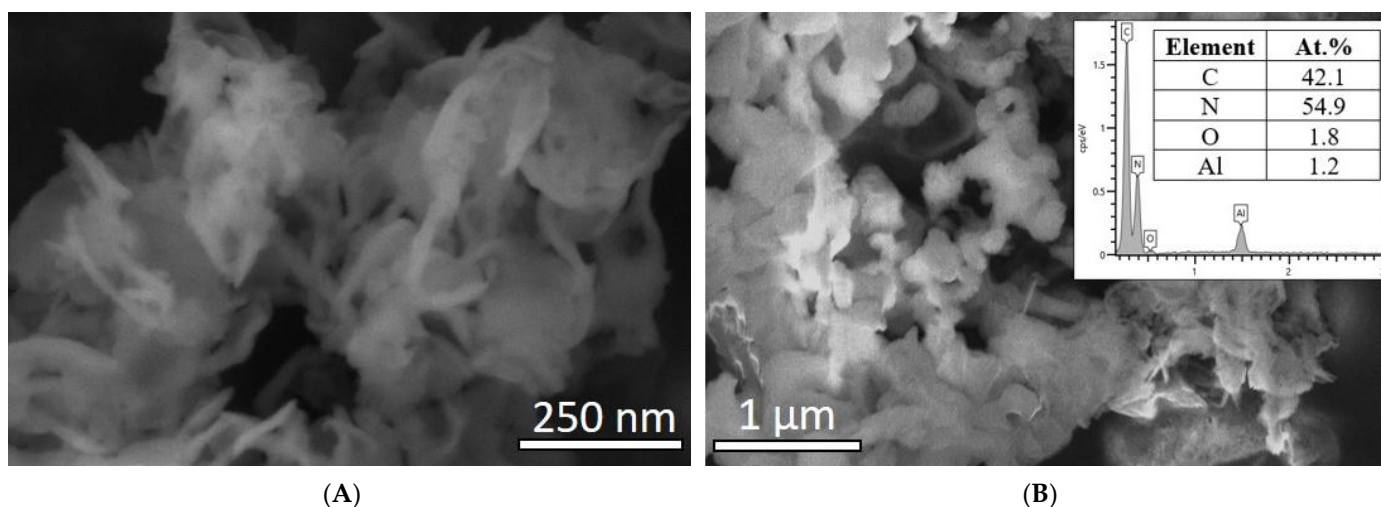


**Figure 6.** (A) SEM image of  $g\text{-C}_3\text{N}_4$  powder and (B) SEM image of immobilised  $g\text{-C}_3\text{N}_4$  on alumina surface along with EDXS conducted over the area.

The results of  $\text{N}_2$  adsorption–desorption isotherm reveal the surface area of around  $88.5 \text{ m}^2/\text{g}$ . With the help of Barret–Joyner–Halenda (BJH) method, the pore diameter was also estimated at 25.8 nm. The obtained result is higher than to the literature findings, based on similar preparation procedures for the  $g\text{-C}_3\text{N}_4$  [31,32].

### 3.2. Photocatalytic Activity of Immobilised $g\text{-C}_3\text{N}_4$ and Its Reusability

Before performing photocatalytic tests, the adhesion of the immobilised photocatalyst on the alumina substrate was investigated. With a single dip into the dispersion, followed by heat treatment for 15 min at  $105^\circ\text{C}$ ,  $g\text{-C}_3\text{N}_4$  bonds to the surface of the ceramic without noticeable peeling. The colour of the disk changes evenly suggesting uniform coverage of the whole disk. Even more, such substrate withstands overnight (total duration of 15 h) magnetic stirring (350 rpm) in ultrapure water with no visual leaching of  $g\text{-C}_3\text{N}_4$  into the water. The stability of immobilised  $g\text{-C}_3\text{N}_4$  was also evident by subsequent UV-Vis analysis initially performed to evaluate catalytic activity. Rayleigh scattering from the possible small residuals, if present in a solution, would intensify an absorption spectrum in the UV part; however, as can be seen from Figure 4B, little if any such elevation was observed. SEM image (Figure 6B) poorly resolves the coverage of alumina substrate probably due to charging and inhomogeneities over the exposed ceramic surface; however, the presence of  $g\text{-C}_3\text{N}_4$  is clearly resolved with EDXS analysis (inset Figure 6B).

The kinetic study is also presented where changes in absorbance were monitored at different time intervals and for different absorption peaks. The degradation of initial concentration ( $10 \text{ mg}\cdot\text{L}^{-1}$ ) was also monitored in pure alumina substrate, the results are also present in Figure 7A (red line).

Following the commonly exploited process for evaluating the degradation rate of MB, the time to reach adsorption-desorption equilibrium by exposing the sample pollutant solutions in the dark was firstly estimated. While the immobilised  $g\text{-C}_3\text{N}_4$  catalyst showed significant adsorption compared to pure alumina initially, MB concentration did not change much after 30 min (and around 15 for pure alumina).

With the onset of photoexcitation,  $g\text{-C}_3\text{N}_4$  immediately starts to further reduce the amount of MB in the solution. The concentration of MB drops to around 20% of the initial value in investigated time interval of 75 minutes. Pure alumina substrate, on the other hand, does not alter the concentration of MB within the next minutes. Small variation in the intensity is probably related to systematic errors introduced by changing sample, refilling the cuvettes etc.

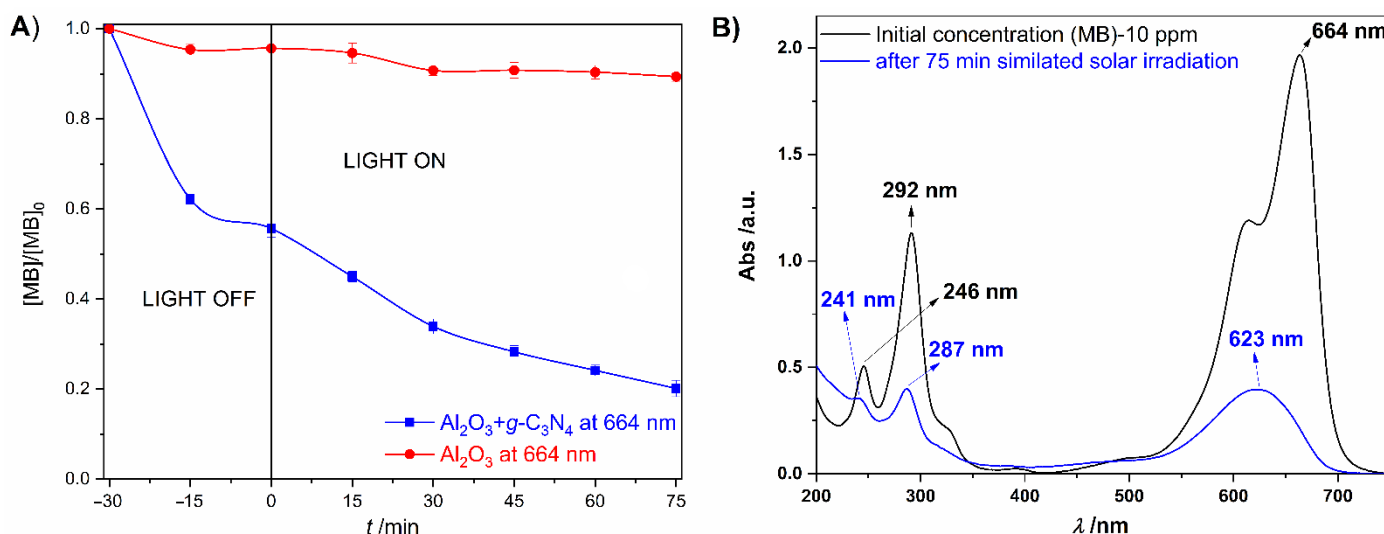


**Figure 7.** (A) Monitoring adsorption and degradation of alumina substrate (red) and immobilised  $g-C_3N_4$  on alumina substrate (blue), and (B) UV-vis absorbance spectra of initial concentration of MB dye and after 75 min photocatalysis.

Adsorption and degradation capabilities of  $g-C_3N_4$  catalyst deposited on alumina substrate for MB photodegradation was investigated by UV-Vis spectroscopy. Degradation of the MB is monitored through the decrease of the absorption spectra characteristic for a given species, Figure 7B. The characteristic peaks of MB at 246 nm, 292 nm, and 664 nm correspond to the chromophore in the structure of MB, N, S substituted heterocycle structure, benzene ring, and dimethylamino group, respectively [33,34].

After 75 min of irradiation under a simulated solar light, all the absorption peaks significantly decreased, Figure 7B, which points to the fact that the chemical structure of MB starts to break. Especially noticeable is the heterocyclic part. All absorption peaks are also shifted to the lower wavelengths at 623, 287, and 241 nm, respectively. Blue shift from 664 nm to 623 nm correspondent to the demethylation of MB structure. The absorption peak at 241 nm corresponding to the aromatic compound suggests that the degradation of MB (using the  $g-C_3N_4$  catalyst) probably produces new metabolites [35]. The pH of the solution plays an important role in the reactive oxygen species (ROS) formation for the photocatalytic degradation of persistent organic contaminants in water [36]. Parameters responsible for the pH changes are substrate and surface chemistry, solvent molecules, catalyst surface charge, types of surface interactions, substrate nature, the extent of adsorption, the numerous intermediates formed during the progress of the reaction, etc. [37]. The pH value of MB initial solution was measured to be around 6.19.

By measuring the whole UV-Vis spectra, it is also possible to distinguish the degradation rate of different chemical bonds. Figure 8A shows the decolourisation (exhibited at 664 nm) and mineralisation (at 292 nm) of MB under irradiation. The photodegradation rate constant ( $k$ ) was calculated from the slope of the time-dependent degradation function in a logarithmic plot, as shown in Figure 8B. The overall rate for both mineralisation and decolourisation is quite different. The decolourisation pseudo-first-order rate constant ( $0.01359 \text{ min}^{-1}$ ) is two times faster in comparison with rate constant of mineralisation ( $0.00621 \text{ min}^{-1}$ ). The obtained linear correlation coefficient ( $R^2$ ) of decolourisation and mineralisation was 0.98796 and 0.99041, respectively; however, the logarithmic plot clearly shows two different kinetics for degradation in both processes. As expected, mineralisation which is slower overall is even slower in the beginning. Within the last 15 min, however, the rate intensifies (green slope Figure 8A) to the same or even larger value as in decolourisation. This furthermore suggests that immobilised  $g-C_3N_4$  photocatalyst on alumina substrate drives decolourisation and mineralisation to faster completion.



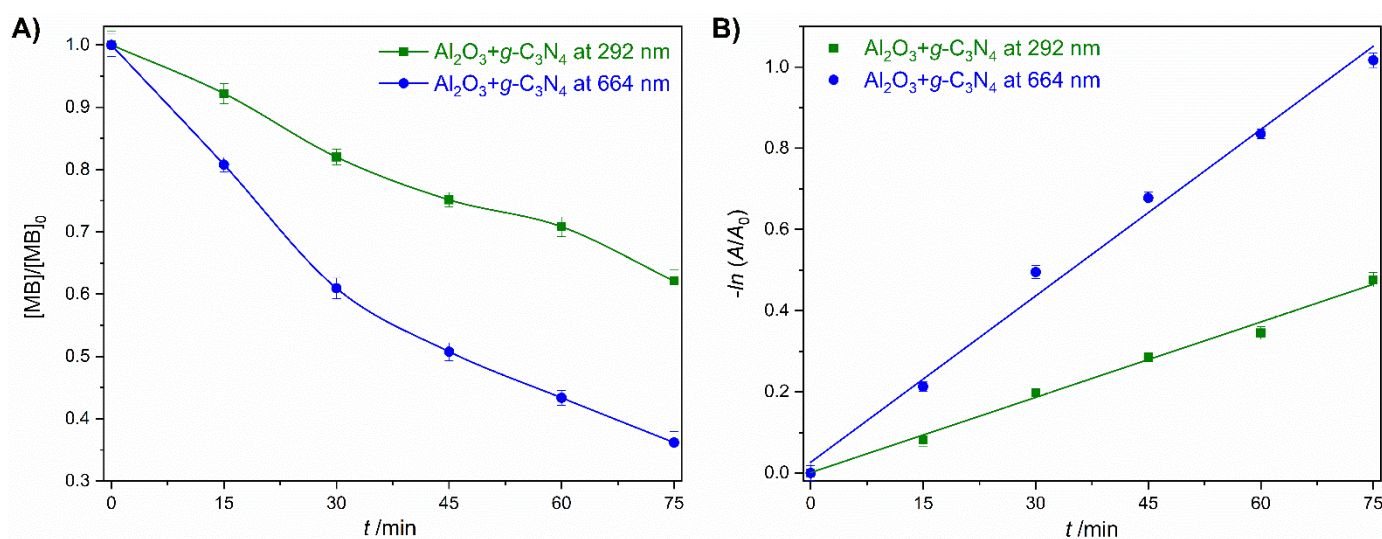


**Figure 8.** (A) Decolourisation (664 nm) and mineralisation (292 nm) of MB as a function of irradiation time under simulated solar irradiation and (B) plotted first-order rate constant ( $k$ ).

Developed CdO/ $Al_2O_3$  nanocomposite by Janani et al. [38] achieved the maximum decolourisation (97.3%) and high mineralisation (87%) in 220 minutes. In another study, copper ferrite particles were co-precipitated onto polydopamine pretreated ceramic/polyester fabrics (CPF) to develop CPF/ $CuFe_2O_4$  photocatalyst. The photocatalytic activity was investigated by degradation of methylene blue (MB), where maximal degradation rate of 98.2% under visible light irradiation for 80 minutes was achieved [39]. Berger et al. [40], anodised aluminium oxide membranes with different pore sizes coated with a titanium dioxide ( $TiO_2$ ) photocatalyst via atomic layer deposition. The photocatalytic membrane cell with active area of  $2\text{ cm}^2$  was used for MB removal. The MB degradation around 50% was achieved in a single-pass flow-through process with possibility to increase the degradation rate by further refinements of the process. In view of this reports our  $g-C_3N_4$  photocatalyst immobilised on alumina substrate demonstrated comparable decolourisation and mineralisation of MB. The photophysical potentials of pure  $g-C_3N_4$  can be modified by heteroatom doping, heterojunction formation by coupling with other materials, and textural modifications to increase the surface area. The improvement or decline of the photocatalytic performance was attributed to the decreased range of the band gap and change in the surface area [41].

Reuse experiments between cycles were presented in Figure 9. The immobilised  $g-C_3N_4$  was reused for several photocatalytic cycles under the same conditions. Between the different cycles, the catalysts were rinsed with ultrapure water and ethanol then dried. Decolourisation of the MB dye (664 nm) as well as mineralisation (292 nm), in comparison between three cycles, is very similar. Decolourisation efficiency of MB was 79.7%, 80.5% and 78.1% after the first, second and third cycles, respectively. Degradation of the aromatic ring was 64.3%, 65.8%, and 64.0% between the cycles. With three cycles, the removal of the aromatic ring is lower in contrast to the decolourisation. The obtained results indicate the high photocatalytic stability of the immobilised  $g-C_3N_4$  on alumina substrate and point towards significant reusability of such setup, which is highly adoptable for various device architectures.

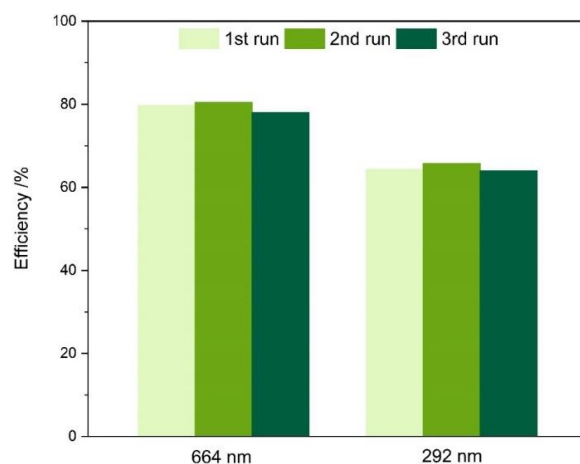


**Figure 9.** Effect of recycling test of immobilised  $g\text{-C}_3\text{N}_4$  on alumina substrate for photocatalytic degradation of MB.

The possible mechanism involved in the degradation of MB dye of the immobilised  $g\text{-C}_3\text{N}_4$  is given schematically in Figure 10. Proposed mechanism presents the explanation of separation of photo-induced electron-hole pairs. When the energy photon ( $h\nu$ ) is absorbed on the  $g\text{-C}_3\text{N}_4$  surface, the electrons ( $e^-$ ) in valence band (VB) absorb photons to get excited and move towards conductive band (CB) leaving positive holes ( $h^+$ ) in VB. Furthermore, electron-hole pairs are produced which play a key role in oxidation and reduction processes. The photocatalytic efficiency of a photocatalyst depends on several crucial factors such as adsorption ability, morphological structure, and charge separation of photo-induced electron-hole pairs [42]. From the oxidation and reduction process hydroxyl ( $\bullet\text{OH}$ ) and superoxide radical ( $\text{O}_2^{\bullet-}$ ) are obtained, respectively, which react with MB dye pollutant to transform MB into non-hazardous compounds such as water and carbon dioxide [43]. A lot of research efforts were put into narrowing the energy bandgap while reducing electron-hole pair's recombination by creating heterojunctions or doping metals into  $g\text{-C}_3\text{N}_4$  as electron entrapment sites, generating highly oxidized holes to efficiently separate holes and electrons; therefore, photocatalytic performance improves [41].

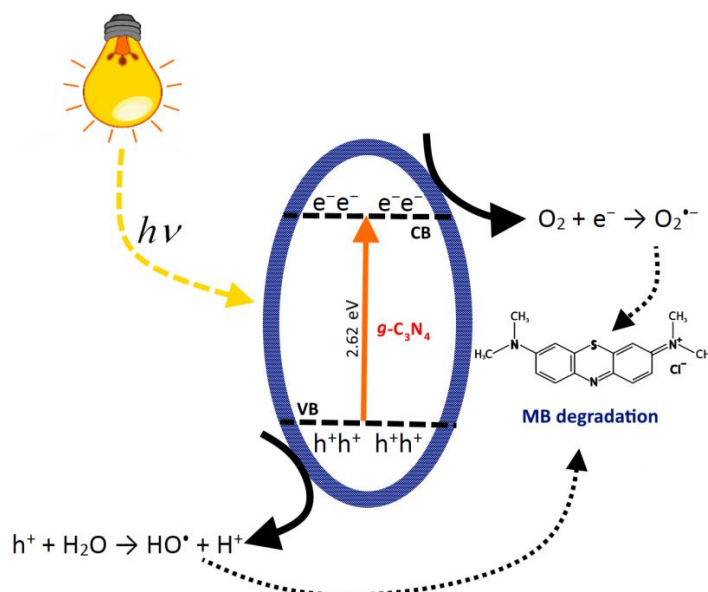


**Figure 10.** The possible mechanism of the photocatalytic degradation of MB at immobilised  $g\text{-C}_3\text{N}_4$  catalyst on the alumina substrate when exposed under simulated solar irradiation.

#### 4. Conclusions

The  $g\text{-C}_3\text{N}_4$  catalyst was successfully prepared by thermal treatment using urea as a precursor at 550 °C in an air chamber and immobilised on an alumina ring substrate. The photocatalytic activity of the immobilised  $g\text{-C}_3\text{N}_4$  catalyst was verified by the photodegradation of methylene blue (MB) dye in an aqueous solution under simulated solar irradiation. The results showed that immobilised  $g\text{-C}_3\text{N}_4$  catalyst shows relatively high adsorption capacity of MB dye in the first 15 min. Further results of the photocatalytic activity show that decolourisation is more than two times faster than mineralisation. After three repetitions of the photocatalytic test, the photodegradation efficiency of MB was still high with negligible deterioration. These results confirmed the stability of the immobilised  $g\text{-C}_3\text{N}_4$  catalyst on the alumina substrate and prove its usefulness due to its simple preparation method, cost-effectiveness, and environmental friendliness.

**Author Contributions:** Conceptualization, M.V., M.K., D.V. and M.P.; methodology, M.V.; software, M.V.; validation, M.V., M.K. and M.P.; formal analysis, M.V.; investigation, M.V. and M.K.; resources, M.P.; data curation, M.V.; writing—original draft preparation, M.V. and M.K.; writing—review and editing, L.Č., T.R., D.V. and M.P.; visualization, M.K. and M.P.; supervision, M.P.; project administration, M.P.; funding acquisition, M.P. All authors have read and agreed to the published version of the manuscript.

**Funding:** This research received no external funding.

**Institutional Review Board Statement:** Not applicable.

**Informed Consent Statement:** Not applicable.

**Data Availability Statement:** Not applicable.

**Acknowledgments:** The financial support of the Slovenian Research Agency is gratefully acknowledged (Project No. L2-1830 and Program No. P2-0084).

**Conflicts of Interest:** The authors declare no conflict of interest.

#### References

1. Danfá, S.; Oliveira, C.; Santos, R.; Martins, R.C.; Quina, M.M.J.; Gomes, J. Development of  $\text{TiO}_2$ -Based Photocatalyst Supported on Ceramic Materials for Oxidation of Organic Pollutants in Liquid Phase. *Appl. Sci.* **2022**, *12*, 7941. [\[CrossRef\]](#)
2. Huang, J.; Puyang, C.; Guo, H. Sodium Percarbonate Activation by Plasma-Generated Ozone for Catalytic Degradation of Dye Wastewater: Role of Active Species and Degradation Process. *Catal.* **2022**, *12*, 681. [\[CrossRef\]](#)
3. Das, S.; Chowdhury, A. Recent advancements of  $g\text{-C}_3\text{N}_4$ -based magnetic photocatalysts towards the degradation of organic pollutants: A review. *Nanotechnology* **2021**, *33*, 72004. [\[CrossRef\]](#)
4. Mahlaule-Glory, L.M.; Hintsho-Mbita, N.C. Green Derived Zinc Oxide (ZnO) for the Degradation of Dyes from Wastewater and Their Antimicrobial Activity: A Review. *Catalysts* **2022**, *12*, 833. [\[CrossRef\]](#)
5. Ahmaruzzaman, M.; Mishra, S.R. Photocatalytic performance of  $g\text{-C}_3\text{N}_4$  based nanocomposites for effective degradation/removal of dyes from water and wastewater. *Mater. Res. Bull.* **2021**, *143*, 111417. [\[CrossRef\]](#)
6. Nemiwal, M.; Zhang, T.C.; Kumar, D. Recent progress in  $g\text{-C}_3\text{N}_4$ ,  $\text{TiO}_2$  and ZnO based photocatalysts for dye degradation: Strategies to improve photocatalytic activity. *Sci. Total Environ.* **2021**, *767*, 144896. [\[CrossRef\]](#)
7. Szczepanik, B. Photocatalytic degradation of organic contaminants over clay- $\text{TiO}_2$  nanocomposites: A review. *Appl. Clay Sci.* **2017**, *141*, 227–239. [\[CrossRef\]](#)
8. Li, X.; Huang, G.; Li, Y.; Chen, X.; Yao, Y.; Liang, Y.; Huang, J.; Zhao, K.; Yin, J. Low-Cost ceramic disk filters coated with Graphitic carbon nitride ( $g\text{-C}_3\text{N}_4$ ) for drinking water disinfection and purification. *Sep. Purif. Technol.* **2022**, *292*, 120999. [\[CrossRef\]](#)
9. Ounas, O.; Lekhlif, B.; Jamal-eddine, J. The facile immobilization of ZnO into a polymer surface for photodegradation of organic contaminants. *Mater. Today Proc.* **2020**, *30*, 816–822. [\[CrossRef\]](#)
10. Chandra Pragada, S.; Thalla, A.K. Polymer-based immobilized  $\text{Fe}_2\text{O}_3\text{-TiO}_2/\text{PVP}$  catalyst preparation method and the degradation of triclosan in treated greywater effluent by solar photocatalysis. *J. Environ. Manag.* **2021**, *296*, 113305. [\[CrossRef\]](#)
11. Liu, S.-H.; Lin, W.-X. A simple method to prepare  $g\text{-C}_3\text{N}_4\text{-TiO}_2$ /waste zeolites as visible-light-responsive photocatalytic coatings for degradation of indoor formaldehyde. *J. Hazard. Mater.* **2019**, *368*, 468–476. [\[CrossRef\]](#) [\[PubMed\]](#)
12. Kumar, A.; Samanta, S.; Srivastava, R. Systematic Investigation for the Photocatalytic Applications of Carbon Nitride/Porous Zeolite Heterojunction. *ACS Omega* **2018**, *3*, 17261–17275. [\[CrossRef\]](#)
13. Mallakpour, S.; Nikkhoo, E. Surface modification of nano- $\text{TiO}_2$  with trimellitylimido-amino acid-based diacids for preventing aggregation of nanoparticles. *Adv. Powder Technol.* **2014**, *25*, 348–353. [\[CrossRef\]](#)

14. Sohrabi, S.; Keshavarz Moraveji, M.; Iranshahi, D. A review on the design and development of photocatalyst synthesis and application in microfluidic reactors: Challenges and opportunities. *Rev. Chem. Eng.* **2020**, *36*, 687–722. [[CrossRef](#)]
15. Gyulavári, T.; Kovács, K.; Kovács, Z.; Bárdos, E.; Kovács, G.; Baán, K.; Magyari, K.; Veréb, G.; Pap, Z.; Hernadi, K. Preparation and characterization of noble metal modified titanium dioxide hollow spheres—New insights concerning the light trapping efficiency. *Appl. Surf. Sci.* **2020**, *534*, 147327. [[CrossRef](#)]
16. Kavitha, R.; Nithya, P.M.; Girish Kumar, S. Noble metal deposited graphitic carbon nitride based heterojunction photocatalysts. *Appl. Surf. Sci.* **2020**, *508*, 145142. [[CrossRef](#)]
17. Bao, Y.; Guo, R.; Gao, M.; Kang, Q.; Ma, J. Morphology control of 3D hierarchical urchin-like hollow  $\text{SiO}_2/\text{TiO}_2$  spheres for photocatalytic degradation: Influence of calcination temperature. *J. Alloys Compd.* **2021**, *853*, 157202. [[CrossRef](#)]
18. Kröger, J.; Jiménez-Solano, A.; Savasci, G.; Lau, V.W.H.; Duppel, V.; Moudrakovski, I.; Küster, K.; Scholz, T.; Gouder, A.; Schreiber, M.-L.; et al. Morphology Control in 2D Carbon Nitrides: Impact of Particle Size on Optoelectronic Properties and Photocatalysis. *Adv. Funct. Mater.* **2021**, *31*, 2102468. [[CrossRef](#)]
19. Wang, R.; Shi, M.; Xu, F.; Qiu, Y.; Zhang, P.; Shen, K.; Zhao, Q.; Yu, J.; Zhang, Y. Graphdiyne-modified  $\text{TiO}_2$  nanofibers with osteoinductive and enhanced photocatalytic antibacterial activities to prevent implant infection. *Nat. Commun.* **2020**, *11*, 4465. [[CrossRef](#)]
20. Wolski, L.; Whitten, J.E.; Sobczak, I.; Ziolek, M. The effect of the preparation procedure on the morphology, texture and photocatalytic properties of ZnO. *Mater. Res. Bull.* **2017**, *85*, 35–46. [[CrossRef](#)]
21. Bai, Z.; Bai, Z.; Gao, T.; Bai, Z.; Zhu, Y. Preparation effects on the morphology and photocatalytic properties of carbon nitride nanotubes. *Results Phys.* **2019**, *13*, 102254. [[CrossRef](#)]
22. Levchuk, I.; Guillard, C.; Dappozze, F.; Parola, S.; Leonard, D.; Sillanpää, M. Photocatalytic activity of  $\text{TiO}_2$  films immobilized on aluminum foam by atomic layer deposition technique. *J. Photochem. Photobiol. A Chem.* **2016**, *328*, 16–23. [[CrossRef](#)]
23. Vukšić, M.; Žmak, I.; Čurković, L.; Čorić, D.; Jenuš, P.; Kocjan, A. Evaluating recycling potential of waste alumina powder for ceramics production using response surface methodology. *J. Mater. Res. Technol.* **2021**, *11*, 866–874. [[CrossRef](#)]
24. Kocijan, M.; Čurković, L.; Bdiķin, I.; Otero-Irurueta, G.; Hortigüela, M.J.; Gonçalves, G.; Radošević, T.; Vengust, D.; Podlogar, M. Immobilised rGO/ $\text{TiO}_2$  Nanocomposite for Multi-Cycle Removal of Methylene Blue Dye from an Aqueous Medium. *Appl. Sci.* **2022**, *12*, 385. [[CrossRef](#)]
25. Kocijan, M.; Čurković, L.; Radošević, T.; Podlogar, M. Enhanced Photocatalytic Activity of Hybrid rGO/ $\text{TiO}_2$ /CN Nanocomposite for Organic Pollutant Degradation under Solar Light Irradiation. *Catalysts* **2021**, *11*, 1023. [[CrossRef](#)]
26. Xing, W.; Tu, W.; Han, Z.; Hu, Y.; Meng, Q.; Chen, G. Template-Induced High-Crystalline  $g\text{-C}_3\text{N}_4$  Nanosheets for Enhanced Photocatalytic  $\text{H}_2$  Evolution. *ACS Energy Lett.* **2018**, *3*, 514–519. [[CrossRef](#)]
27. Su, Q.; Sun, J.; Wang, J.; Yang, Z.; Cheng, W.; Zhang, S. Urea-derived graphitic carbon nitride as an efficient heterogeneous catalyst for  $\text{CO}_2$  conversion into cyclic carbonates. *Catal. Sci. Technol.* **2014**, *4*, 1556–1562. [[CrossRef](#)]
28. Wang, S.; Wang, F.; Su, Z.; Wang, X.; Han, Y.; Zhang, L.; Xiang, J.; Du, W.; Tang, N. Controllable Fabrication of Heterogeneous p- $\text{TiO}_2$  QDs@ $g\text{-C}_3\text{N}_4$  p-n Junction for Efficient Photocatalysis. *Catalysts* **2019**, *9*, 439. [[CrossRef](#)]
29. Narkbuakaew, T.; Sujaridworakun, P. Synthesis of Tri-S-Triazine Based  $g\text{-C}_3\text{N}_4$  Photocatalyst for Cationic Rhodamine B Degradation under Visible Light. *Top. Catal.* **2020**, *63*, 1086–1096. [[CrossRef](#)]
30. Chen, X.; Kuo, D.-H.; Lu, D. Nanonization of  $g\text{-C}_3\text{N}_4$  with the assistance of activated carbon for improved visible light photocatalysis. *RSC Adv.* **2016**, *6*, 66814–66821. [[CrossRef](#)]
31. Wang, H.; Zhang, X.; Xie, J.; Zhang, J.; Ma, P.; Pan, B.; Xie, Y. Structural distortion in graphitic- $\text{C}_3\text{N}_4$  realizing an efficient photoreactivity. *Nanoscale* **2015**, *7*, 5152–5156. [[CrossRef](#)] [[PubMed](#)]
32. Li, H.J.; Sun, B.W.; Sui, L.; Qian, D.J.; Chen, M. Preparation of water-dispersible porous  $g\text{-C}_3\text{N}_4$  with improved photocatalytic activity by chemical oxidation. *Phys. Chem. Chem. Phys.* **2015**, *17*, 3309–3315. [[CrossRef](#)] [[PubMed](#)]
33. Wu, K.; Shi, M.; Pan, X.; Zhang, J.; Zhang, X.; Shen, T.; Tian, Y. Decolourization and biodegradation of methylene blue dye by a ligninolytic enzyme-producing *Bacillus thuringiensis*: Degradation products and pathway. *Enzyme Microb. Technol.* **2022**, *156*, 109999. [[CrossRef](#)] [[PubMed](#)]
34. Sun, Y.; Cheng, S.; Lin, Z.; Yang, J.; Li, C.; Gu, R. Combination of plasma oxidation process with microbial fuel cell for mineralizing methylene blue with high energy efficiency. *J. Hazard. Mater.* **2020**, *384*, 121307. [[CrossRef](#)]
35. Miao, S.; Liu, Z.; Han, B.; Zhang, J.; Yu, X.; Du, J.; Sun, Z. Synthesis and characterization of  $\text{TiO}_2$ -montmorillonite nanocomposites and their application for removal of methylene blue. *J. Mater. Chem.* **2006**, *16*, 579–584. [[CrossRef](#)]
36. Pelaez, M.; Falaras, P.; Likodimos, V.; O'Shea, K.; de la Cruz, A.A.; Dunlop, P.S.M.; Byrne, J.A.; Dionysiou, D.D. Use of Selected Scavengers for the Determination of NF- $\text{TiO}_2$  Reactive Oxygen Species during the Degradation of Microcystin-LR under Visible Light Irradiation. *J. Mol. Catal. A Chem.* **2016**, *425*, 183–189. [[CrossRef](#)]
37. John, D.; Rajalakshmi, A.S.; Lopez, R.M.; Achari, V.S.  $\text{TiO}_2$ -reduced graphene oxide nanocomposites for the trace removal of diclofenac. *SN Appl. Sci.* **2020**, *2*, 840. [[CrossRef](#)]
38. Janani, B.; Syed, A.; Raju, L.L.; Bahkali, A.H.; Al-Rashed, S.; Elgorban, A.M.; Ahmed, B.; Thomas, A.M.; Khan, S.S. Designing intimate porous  $\text{Al}_2\text{O}_3$  decorated 2D CdO nano-heterojunction as enhanced white light driven photocatalyst and antibacterial agent. *J. Alloys Compd.* **2022**, *896*, 162807. [[CrossRef](#)]
39. Cheng, D.; Yan, C.; Liu, Y.; Zhou, Y.; Lu, D.; Tang, X.; Cai, G.; Li, D.; Zhao, Z.; Wang, X. Loading  $\text{CuFe}_2\text{O}_4$  onto ceramic fabric for photocatalytic degradation of methylene blue under visible light irradiation. *Ceram. Int.* **2022**, *48*, 1256–1263. [[CrossRef](#)]



40. Berger, T.E.; Regmi, C.; Schäfer, A.I.; Richards, B.S. Photocatalytic degradation of organic dye via atomic layer deposited TiO<sub>2</sub> on ceramic membranes in single-pass flow-through operation. *J. Memb. Sci.* **2020**, *604*, 118015. [[CrossRef](#)]
41. Palani, G.; Apsari, R.; Hanafiah, M.M.; Venkateswarlu, K.; Lakkaboyana, S.K.; Kannan, K.; Shivanna, A.T.; Idris, A.M.; Yadav, C.H. Metal-Doped Graphitic Carbon Nitride Nanomaterials for Photocatalytic Environmental Applications—A Review. *Nanomaterials* **2022**, *12*, 1754. [[CrossRef](#)] [[PubMed](#)]
42. Aslam, I.; Hassan Farooq, M.; Ghani, U.; Rizwan, M.; Nabi, G.; Shahzad, W.; Boddula, R. Synthesis of novel g-C<sub>3</sub>N<sub>4</sub> microrods: A metal-free visible-light-driven photocatalyst. *Mater. Sci. Energy Technol.* **2019**, *2*, 401–407. [[CrossRef](#)]
43. Molaei, P.; Rahimi-Moghadam, F. Porous g-C<sub>3</sub>N<sub>4</sub> nanosheets through facile thermal polymerization of melamine in the air for photocatalyst application. *J. Mater. Sci. Mater. Electron.* **2021**, *32*, 19655–19666. [[CrossRef](#)]